Acta Oceanol. Sin., 2015, Vol. 34, No. 12, P. 80–92
DOI: 10.1007/s13131-015-0773-x
http://www.hyxb.org.cn
E-mail: hyxbe@263.net

Variability of sea surface height in the South China Sea and its relationship to Pacific oscillations

PEI Yuhua[1, 2*], ZHANG Rong-Hua[3], ZHANG Xiangming[2], JIANG Lianghong[2], WEI Yanzhou[3]

[1] College of Oceanic and Atmospheric Sciences, Ocean University of China, Qingdao 266100, China

[2] State Key Laboratory of Satellite Ocean Environment Dynamics, Second Institute of Oceanography, State Oceanic Administration, Hangzhou 310012, China

[3] Key Laboratory of Ocean Circulation and Waves, Institute of Oceanology, Chinese Academy of Sciences, Qingdao 266071, China

Received 6 March 2015; accepted 7 May 2015

Abstract

The spatio-temporal variability modes of the sea surface height in the South China Sea (SCS-SSH) are obtained using the Cyclostationary Empirical Orthogonal Function (CSEOF) method, and their relationships to the Pacific basin scale oscillations are examined. The first CSEOF mode of the SCS-SSH is a strongly phase-locked annual cycle that is modulated by a slowly varying principal component (PC); the strength of this annual cycle becomes reduced during El Niño events (at largest by 30% off in 1997/98) and enhanced during La Niña events. The second mode is a low frequency oscillation nearly on decadal time scale, with its spatial structure exhibiting an obscure month-dependence; the corresponding PC is highly correlated with the Pacific Decadal Oscillation (PDO) index. Five independent oscillations in the Pacific are isolated by using the independent component (IC) analysis (ICA) method, and their effects on the SCS-SSH are examined. It is revealed that the pure ENSO mode (which resembles the east Pacific ENSO) has little effect on the low frequency variability of the SCS-SSH while the ENSO reddening mode (which resembles the central Pacific ENSO) has clear effect. As the ENSO reddening mode is an important constituent of the PDO, this explains why the PDO is more important than ENSO in modulating the low frequency variability of SCS-SSH. Meridional saddle like oscillation mode, the Kuroshio extension warming mode, and the equatorial cooling mode are also successfully detected by the ICA, but they have little effect on the low frequency variability of the SCS-SSH. Further analyses suggest the Pacific oscillations are probably influencing the variability of the SCS-SSH in ways that are different from that of the sea surface temperature (SST) in the SCS.

Key words: South China Sea, sea surface height, ENSO, PDO

Citation: Pei Yuhua, Zhang Rong-Hua, Zhang Xiangming, Jiang Lianghong, Wei Yanzhou. 2015. Variability of sea surface height in the South China Sea and its relationship to Pacific oscillations. Acta Oceanologica Sinica, 34(12): 80–92, doi: 10.1007/s13131-015-0773-x

1 Introduction

The South China Sea (SCS) is a marginal sea semi-enclosed by China, Philippines, Vietnam, and Brunei, and is connected to the Pacific Ocean through the Luzon Strait. Due to its geographic location, the variability of the sea surface height in the SCS (SCS-SSH) is influenced by the East Asian Monsoon and the Pacific basin-scale climate oscillations, and hence displays seasonal and interannual variability characteristics (e.g., Ho et al., 2000; Zhou et al., 2012). The distribution pattern of the SCS-SSH generally reflects the upper ocean circulation in the SCS; therefore, examining its variability and relationships to the Pacific oscillations can help better understand the variability of ocean circulation on one hand, and the interaction and exchanges between the SCS and the Pacific Ocean on the other hand.

Generally, the SCS-SSH is low in the central SCS basin and high along the continental shelf (as indicated in Fig. 1a), accompanied by significantly spatio-temporal variability (e.g., Wu et al., 1998; Fang et al., 2006; Zhou et al., 2012). As indicated from the standard deviation (SD) of the SCS-SSH (Fig. 1a), the SCS-SSH displays large spatial variability at the western coast of the SCS and the middle SCS basin to the west of Luzon Strait and to the southeast of Vietnam. Accompanied with its spatial variability, the SCS-SSH also displays annual and interannual variability, as indicated by the time series of the domain-averaged SCS-SSH anomaly in Fig. 1b.

The spatio-temporal variability modes of the SCS-SSH were commonly detected by using the Empirical Orthogonal Function (EOF) method (North, 1984). Zheng et al. (2007) applied the EOF method to the monthly SCS-SSH data and found that the largest variability amplitude of the principal mode was located on the western SCS. Fang et al. (2006) and Zhou et al. (2012) applied the EOF method to the 12-month and 13-month low-pass filtered SCS-SSH data respectively, and found that the largest variability amplitude of the principal mode was located at the eastern SCS basin in vicinity to the Philippines. The scale-reliant oscillation patterns are caused by the different physical processes involved.

Foundation item: The National Natural Science Foundation of China under contract Nos 91128204, 41321004, 41475101 and 41421005; the National Basic Research Program (973 Program) of China under contract No. 2013CB430302; the Natural Science Foundation of China-Shandong Joint Fund for Marine Science Research Centers under contract No. U1406401; the Strategic Priority Project of Chinese Academy of Sciences under contract Nos XDA11010301 and XDA11010104.

*Corresponding author, E-mail: pei.yuhua@hotmail.com

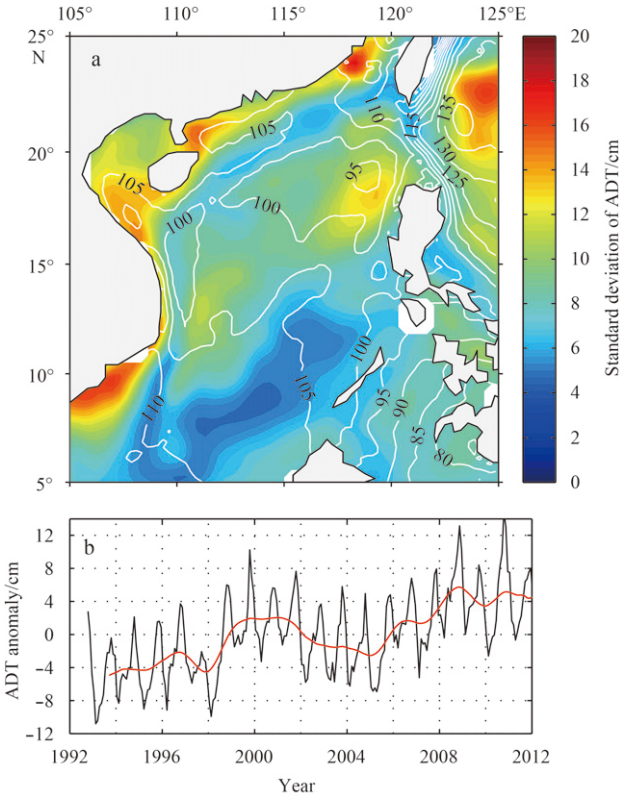

Fig. 1. The climatological mean (white contour lines) and standard deviation (superimposed with colors) of the absolute dynamic height (ADT) in the South China Sea (a); the time series of the SCS domain-averaged monthly ADT anomaly (black line) and that smoothed by 13-month moving average (red line) (b).

Specifically, the annual cycle is related to monsoon, while the interannual-decadal variability is related to the El Niño-Southern Oscillation (ENSO) and the Pacific Decadal Oscillation (PDO) (e.g., Wu et al., 1998; Fang et al., 2006; Zhou et al., 2012). However, as the EOF method was not suitable to detect the non-stationary oscillations that were ubiquitous in nature (Kim and North, 1997; Kim and Wu, 1999), the inherent oscillating modes in the SCS-SSH may suffer from the mode-splitting problem. For example, the inherent annual variability signal may be split and distributed to different EOF modes. To solve this mode-splitting problem, the cyclostationary EOF (CSEOF) method, which can capture the slow modulations of phase-locked annual cycles, was proposed by Kim and North (1997). In this study, this method is used to investigate the spatio-temporal variability modes of the SCS-SSH.

The ENSO and PDO act to exert significant influences on the low frequency variability in the SCS. For instance, they can influence the bifurcation of the North Equatorial Current and further the transport through the Mindoro Strait and the Luzon Strait, as well as the East Asian Monsoon and the circulation in the SCS (e.g., Qiu and Lukas, 1996; Qu et al., 2004; Wang et al., 2006; Liu et al, 2011; Zhou et al., 2012). The relationship between interannual-decadal variability of the SCS-SSH and ENSO (or PDO) was generally established from the high correlation between the EOF principal component of the SCS-SSH and the ENSO (or PDO) index, or by examining the anomalous features of the SSH or circulation in different phases of the ENSO (e.g., Chao et al., 1996; Qiu et al., 2012). However, the roles of ENSO and PDO in modulating the SCS-SSH are rarely distinguished, and which plays a dominant role in modulating the lower frequency oscillation of the SCS-SSH is still in debate. For example, Qiu et al. (2012) noticed that the lower frequency variability of the SCS-SSH is related to ENSO, while Wu (2013) noticed that the PDO played a more important role than ENSO. This study will show that the ENSO and PDO are linked to the first and second CSEOF modes respectively.

The ambiguity between the effects of ENSO and PDO in modulating the SCS-SSH lays on the high similarity between their indices. However, the ENSO represents the interannual oscillation in the tropical Pacific, while the PDO represents the interannual to decadal oscillations in the North Pacific. The similarity between the two indices suggests there are interconnections between the tropical and subtropical variability in the Pacific (e.g., Zhang and Levitus, 1997; Zhang et al., 1998). Clearly, taking the tropical Pacific and North Pacific together as a whole, and separating the independent source oscillations in this big area are desirable for further examining their effects on the low frequency variability of the SCS-SSH. The effects of different Pacific oscillation modes on the SCS-SSH are reported in this study.

In this study, the CSEOF method is firstly applied to detect the spatio-temporal variability modes of the SCS-SSH. As shall be seen below, the inherent annual cycle mode and low frequency oscillation mode can be both successfully detected in a concise way. Correlation analyses indicate these two modes are linked to ENSO and PDO respectively. Pacific independent oscillation modes are detected by using the independent component (IC) analysis (ICA) method (Hyvärinen and Oja, 2000), and their effects on the low frequency variability of the SCS-SSH are examined. Following these analyses, the difference between ENSO and PDO in modulating the variability in the SCS is discussed.

2 Data and methods

2.1 *Data*

To explore the spatio-temporal variability of the SCS-SSH and their relationships to the Pacific basin scale oscillations, the satellite altimeter data, the sea surface temperature (SST) data, ENSO index, and PDO index are used in this study.

The satellite altimeter data are from the Ssalto/Duacs gridded absolute dynamic topography (ADT) & absolute geostrophic velocities products. The SSH is defined as the sum of the ADT with a constant geoid. The satellite altimeter data were produced by Ssalto/Duacs system and distributed by Aviso with support from Cnes (http://www.aviso.altimetry.fr/duacs/), which are available from October 1992 to the present. These satellite altimetry products are merged from all altimeter missions, Saral, Cryosat-2, Jason-1&2, T/P, Envisat, GFO, ERS-1&2 and even Geosat. The spatial resolution is (1/3)°×(1/3)° with global coverage, and the temporal resolution is one week. The ADT data used in this study were taken from the products from October 1992 to April 2012, and the weekly data were processed to monthly data by taking average of the samples in the same month of a year.

The SST data are taken from the Met Office Hadley Centre Sea Ice and Sea Surface Temperature data set (HadISST) (Rayner et al., 2003), and downloaded from the Met Office Hadley Centre (http://www.metoffice.gov.uk/hadobs/). The HadISST data set provides global monthly fields of SST on a 1-degree latitude-longitude grid from 1870 to date.

The ENSO index from 1868 to 2012 used in this study is devised by the Japan Meteorological Agency (JMA), which is a SST-based index for determining El Niño and La Niño events. This in-

dex selects well the known ENSO events, and is available via http://coaps.fsu.edu/pub/JMA_SST_Index/. The ENSO index is computed based on reconstructed monthly mean SST fields for the period January 1868 to February 1949, and on observed JMA SST index for March 1949 to present. The reconstructed SST fields were computed using an orthogonal projection technique (Meyers et al., 1999). The ENSO index is a 5-month running mean of spatially averaged SST anomalies over the tropical Pacific: 4°S–4°N, 150°–90°W. If index values are 0.5°C or greater for 6 consecutive months (including October-November-December (OND)), the ENSO year of October through the following September is categorized as El Niño, La Niña (index values equal or exceed –0.5°C), or as neutral (all other values).

The PDO index is defined as the leading principal component of monthly SST anomalies in the North Pacific Ocean, poleward of 20°N (Mantua et al., 1997; Zhang et al., 1997). The monthly PDO index is available from 1900 to present, which can be downloaded from http://jisao.washington.edu/pdo/PDO.latest.

2.2 *Methods*

The CSEOF method proposed by Kim and North (1997) was used to detect the spatio-temporal variability modes of the SCS-SSH. The CSEOF method can be used to decompose the space-time field $T(\vec{r},t)$ into multiplications of cyclostationary loading vectors (CSLVs) and corresponding principal components (PCs) like that:

$$T(\vec{r},t)=\sum_i PC_i(t)\cdot CSLV_i(\vec{r},t), \tag{1}$$

where $PC_i(t)$ and $CSLV_i(\vec{r},t)$ denote the temporal and spatial components of the i-th CSEOF mode respectively. The CSEOF modes are sorted according to their relative importance in explaining the total variance of $T(\vec{r},t)$. In contrast to classical EOF method, the spatial mode from CSEOF varies with time at a nest period d (taken 12 months in this study), i.e.,

$$CSLV_i(\vec{r},t+d)=CSLV_i(\vec{r},t). \tag{2}$$

Each $CSLV_i(\vec{r},t)$ represents a nested physical evolution, and the corresponding $PC_i(t)$ reflects varying strength of this evolution. The CSEOF method can capture moving oscillation patterns, while the EOF method is suitable to detect the stationary patterns (Kim and Wu, 1999). It inherits the advantage of S-EOF method (Wang and An, 2005) in detecting the season-reliant oscillation patterns, while keeps the time resolution of PCs identical to that of samples. It is also capable of resolving the spatial evolution under a nest period d and the temporal modulation as that can be obtained by using the ensemble empirical mode decomposition and the multichannel singular spectrum analysis methods (Zhu et al., 2012).

The ICA method is used to separate the mixtures of the signals in the Pacific Ocean into their independent sources. Similar to the EOF method, it decomposes a space-time field $T(\vec{r},t)$ into multiplications of space field $S_i(\vec{r})$ with time component $IC_i(t)$ like that:

$$T(\vec{r},t)=\sum_i IC_i(t)\cdot S_i(\vec{r}). \tag{3}$$

However, this method has a more strict restriction than the traditional EOF method on that the time modes $IC_i(t)$ are restricted to be independent rather than uncorrelated. As evaluated by Aires et al. (2002) and Hannachi et al. (2009), the ICA method can work better than both EOF and rotated EOF (REOF) method in meteorological studies. Therefore, it is chosen to detect the independent oscillation modes in the Pacific in this study. A FastICA program, which is coded based on the Hyvärinen's fixed-point algorithm (Hyvärinen and Oja, 2000), is employed in this study. In practice, in order to reduce the data redundancy and increase the computation speed, the principal component analysis (PCA) is firstly applied to the data, and a certain number of the leading PCA modes are retained for doing the ICA.

3 Results

3.1 *The spatio-temporal variability of the SCS-SSH*

The normal annual cycle of the SCS-SSH and the sea surface circulation are drawn in Fig. 2. The SCS-SSH is generally high in summer and autumn while low in winter and spring. However, affected by monsoon, the SSH does not evolve in-phase in the whole SCS. The seasonal variability of the circulation is characterized by a cyclonic circulation in the northern SCS in winter while an anti-cyclonic circulation in the southern SCS in summer, which is consistent to previous observations (Hu et al., 2000; Su, 2004).

The CSEOF modes of the SCS-SSH can depict how its variance is explained and how the annual cycle is modulated by the low frequency variability. The two leading CSEOF modes, which explain 45.38% and 18.97% of the total variance of the SCS-SSH respectively, are shown in Figs 3 and 4.

The first CSLV shows the normal annual cycle of the SCS-SSH anomaly. Its corresponding PC oscillates around 1.0 without changing sign, meaning the annual cycle of the SCS-SSH is generally stable without reversing phase. The annual cycle of the SCS-SSH varies by about ±20 cm (Fig. 3a), which is in agreement with the SD values that are observed in the SCS (Fig. 1a). Along the west continental shelf of the SCS, the large amplitude of the annual cycle explains the significant SD as shown in Fig. 1a. The amplitude of the annual cycle increases when the PC exceeds 1.0 (at about 1.2 to the most) while deceases when the PC drops below 1.0 (at 0.7 to the least).

The second CSLV displays negative values in most areas of the SCS for all the 12 months, especially in the southeast of the SCS (Fig. 4a). The spatial patterns from the 12-month results are similar with each other if looking over from a global point of view, despite some clear differences exist locally, e.g., the significant negative value to the east of Vietnam appears in September while disappears in some other months. This CSEOF mode represents month-reliant response of the SCS-SSH to the low frequency modulation. The larger CSLV value in the southeastern SCS means the SSH in this position is more sensitive to low frequency modulation.

Power spectra of the PCs, which are derived using an auto-regressive (AR) model, are shown in Fig. 5a. Results indicate the first mode is dominated by an interannual variability at a period of 3.6 a, while the second mode is dominated by a near-decadal variability at a period of 7.1 a and an interannual variability at a period of 2.4 a. Therefore, the SCS-SSH is modulated by both interannual and near-decadal oscillations.

The correlation coefficient between PC1 and PC2 is 0.30. That means when the SSH in the SCS is high (or PC2 is low), the annual cycle would get enhanced (PC1 is high). It should be noticed that the CSEOF decomposition only requires the scalar product

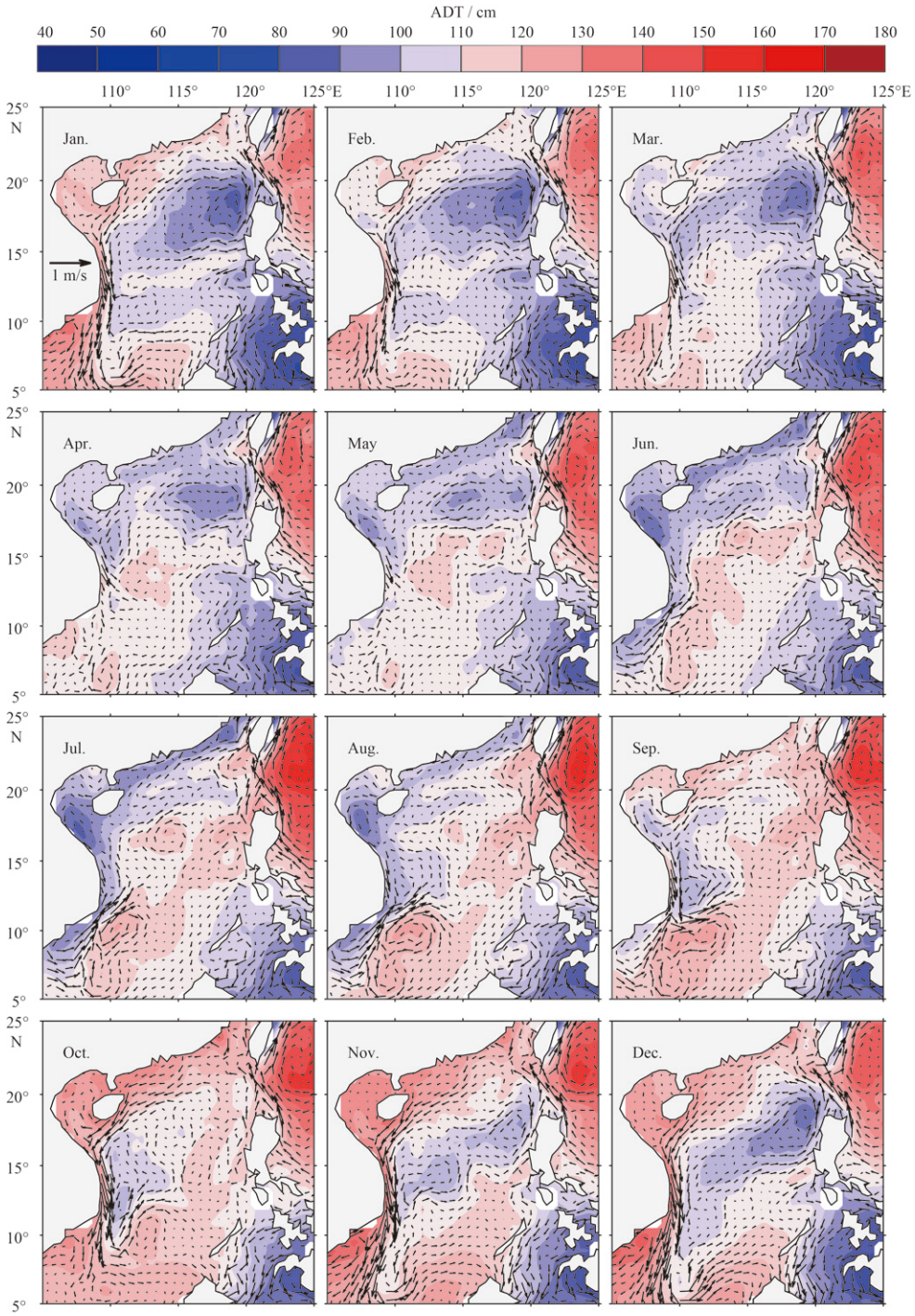

Fig. 2. Monthly mean climatology of the ADT and surface absolute geostrophic velocities in the South China Sea.

between two PCs to be zero, while not their correlation coefficient.

3.2 *The independent oscillations in the Pacific*

As the SCS is a marginal sea which connected to the Pacific Ocean, the variability in the Pacific can exert significant influences on the low frequency variability in the SCS through the Luzon Strait and the Mindoro Strait. In order to explore the relationship between the spatio-temporal variability modes of the SCS-SSH and the low-frequency oscillations in the Pacific, the independent source oscillations in the Pacific are firstly isolated. Previously, some climatic variability modes in the Pacific have been detected by analyzing the long term SST data. They include the most well-known interannual variability signal ENSO in the tropical Pacific, which is further divided into the East Pacific (EP) type and the Central Pacific (CP) type (Ashok et al., 2007; Kao and Yu, 2009), and the PDO centered in the North Pacific (Mantua et al., 1997; Zhang et al., 1997). The enhanced warming over the subtropical western boundary current (Wu et al., 2012) and the cooling in the tropical Pacific (Cane et al., 1997; Deser et al., 2010; Zhang et al., 2010) were also observed. Correctly detecting these modes and defining their variability indices have profound signi-

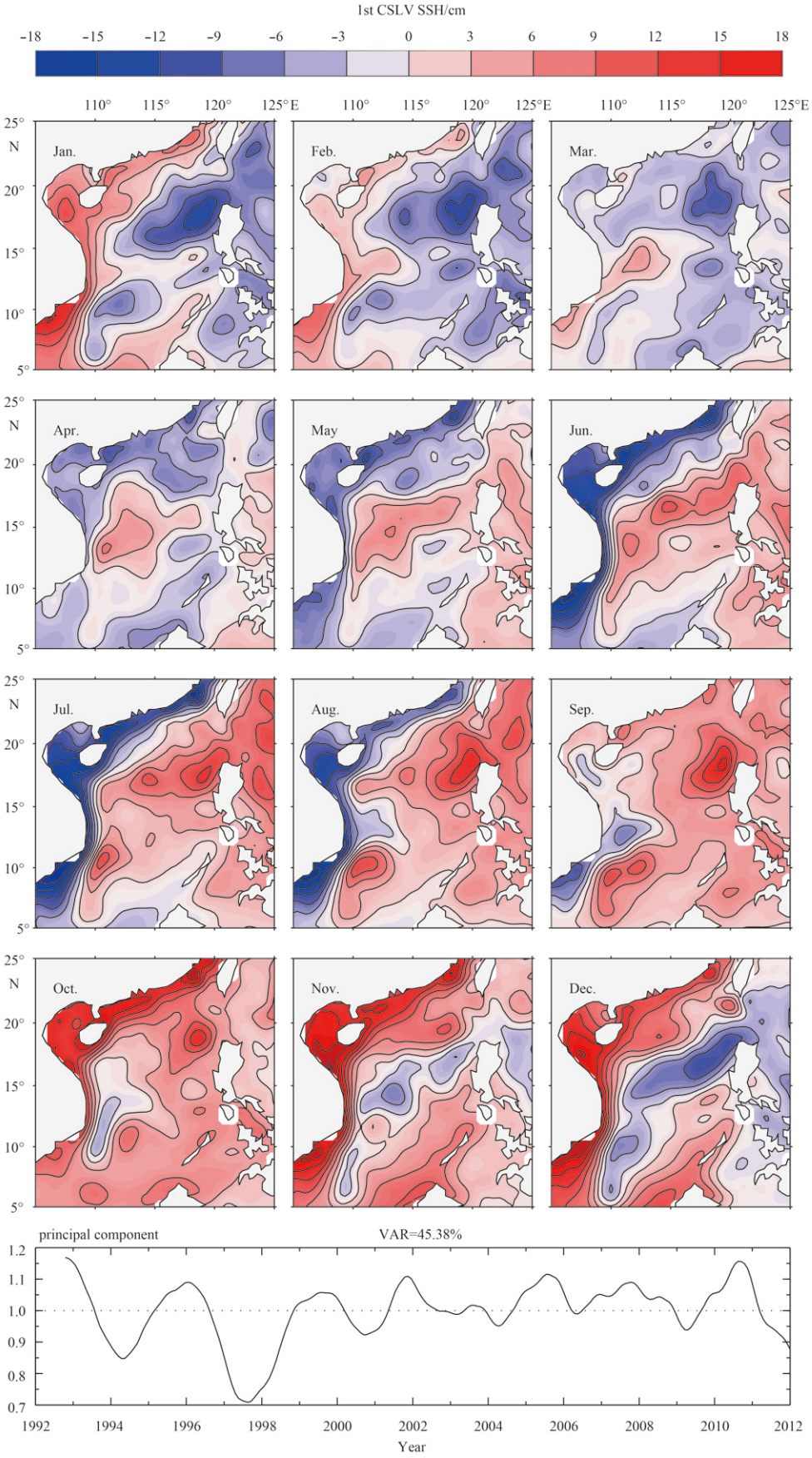

Fig. 3. The first CSEOF mode of the SSH in the SCS. The 12-month spatial patterns represent a cyclostationary loading vector, while the black line displayed at the bottom panel represents the principal component.

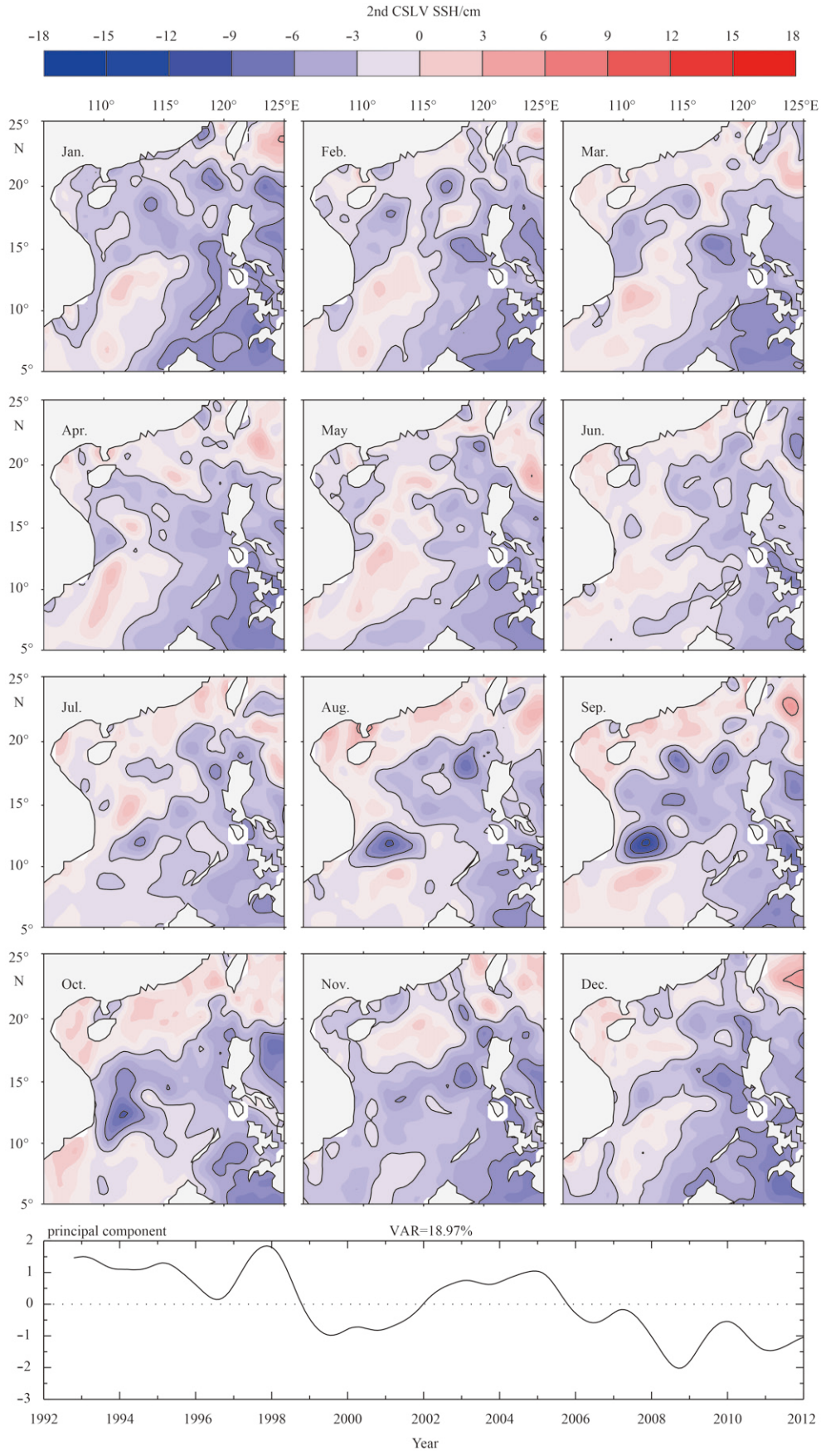

Fig. 4. The second CSEOF mode of the SSH in the SCS. The 12-month patterns represent a cyclostationary loading vector, while the black line displayed at the bottom panel represents the principal component.

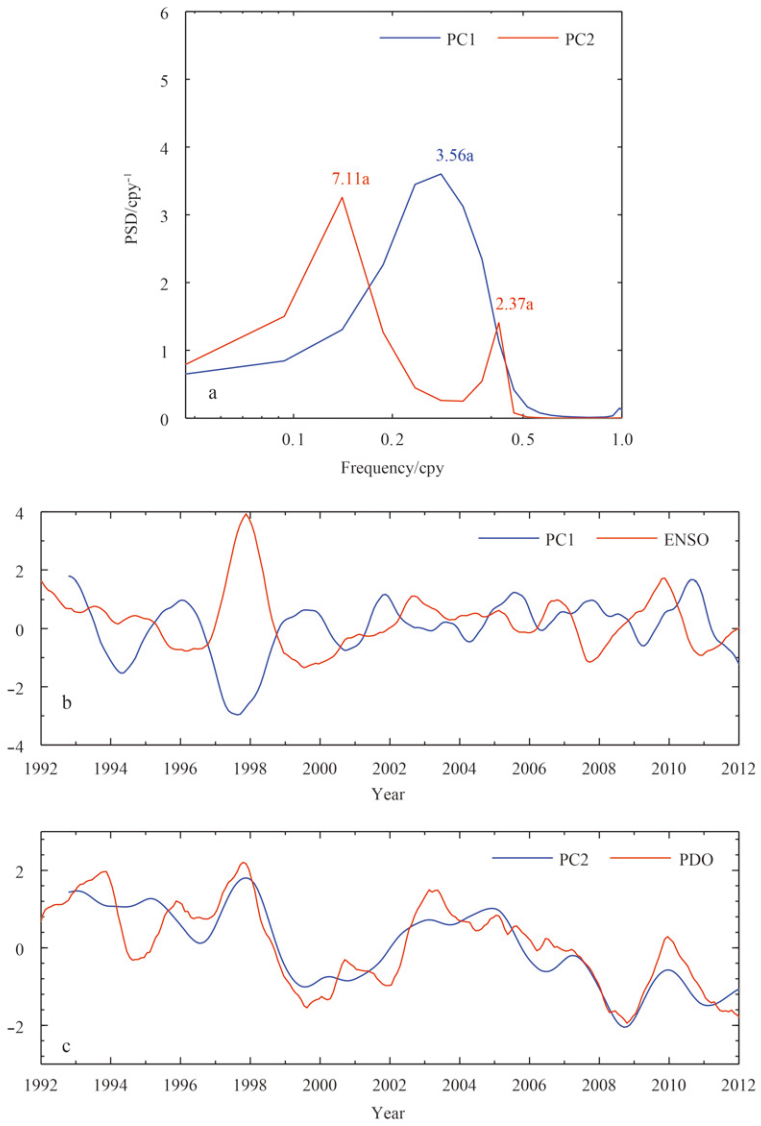

Fig. 5. The power spectra of the first and second PCs of the SCS-SSH (a), the comparison of the first PC of the SCS-SSH with the ENSO index (b), and the comparison of second PC of the SCS-SSH with the PDO index (c).

ficance in the climate research. However, these previously observed modes were obtained using different approaches, with some modes often being correlated with each other (e.g., the ENSO and the PDO share a high similarity). Therefore, isolating the intrinsic independent oscillations in the Pacific is desirable.

To approach the above goal, the ICA method is adopted in this work. As these previously derived modes were all obtained from SST data, for consistency, the ICs in the Pacific basin are also defined from the SST data. Before carrying out the ICA method, the SST data are low-pass filtered by using Fast Fourier Transform (FFT) and inverse FFT (iFFT) methods, with the frequency components exceed 0.8 cpy (cycle per year) being filtered out. The first 10 PCs, which explain 88% of the variance altogether, are left to do rotation to obtain the ICs. Finally, there are 5 ICs are derived, as shown in Fig. 6.

The 1st IC is characterized by a classical El Niño oscillation pattern. As inferred from the spatial mode, the warming in the eastern tropical Pacific is accompanied by a simultaneous warming in the west Pacific along the marginal seas that includes the SCS. That means this mode has a clear effect on the low frequency variability of the SST in the SCS. This mode was often termed as the EP El Niño mode or cold tongue El Niño mode (Kao and Yu, 2009; Kug et al., 2009). The time series of the 1st mode suggests that there were two extremely strong EP El Niño events in the years 1982/83 and 1997/98, which is well consistent with the historical observations.

The 2nd IC is characterized by an ENSO reddening pattern, which resembles a westward propagated and fainted signal from a strong oscillation in the EP. As evident from the spatial pattern, this mode has little effect on the SST in the west Pacific and the SCS. The spatial mode resembles to that of the so-called El Niño Modoki (Ashok et al., 2007), CP El Niño (Kao and Yu, 2009), or warm pool El Niño (Kug et al., 2009), but their time modes are not necessarily identical. To distinguish it from the previous ones, we call it the ENSO-reddening mode.

The 3rd IC reflects a horse saddle like spatial distribution pattern from tropics, bypass subtropics, to the mid-latitude. This mode agrees with the fact that the warming in the mid-latitude

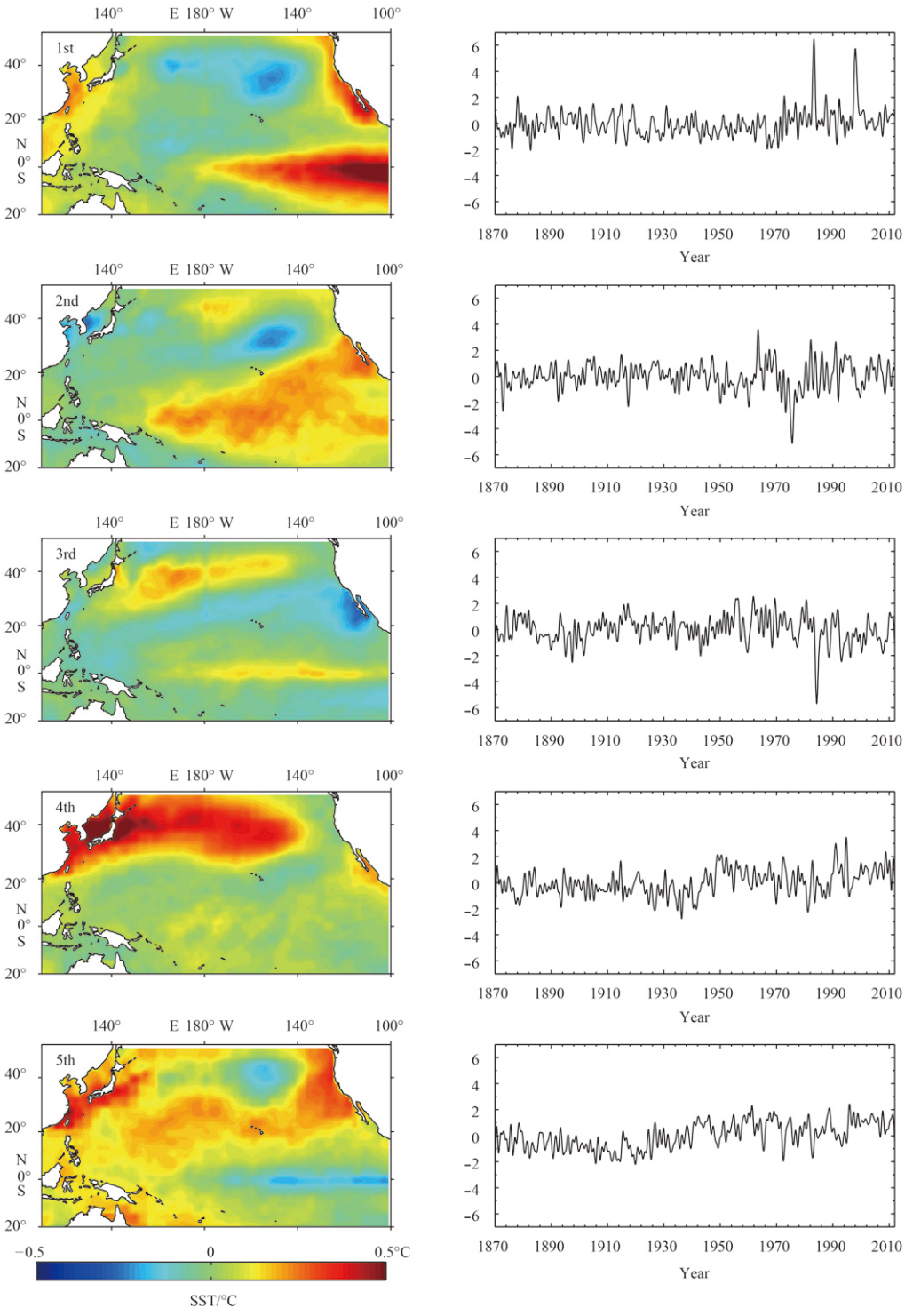

Fig. 6. Independent Pacific oscillations derived from SST using the ICA method.

can penetrate through the subtropics through ocean subsurface layer or from an atmospheric bridge to affect SST in the tropics (Zhang et al., 1998; Lau and Nath, 1996; Alexander et al., 2002).

The 4th IC depicts the warming at the Kuroshio extension region. This result is in accordance with the enhanced warming in the global subtropical western boundary current domain as observed by Wu et al. (2012). It can be seen that the mostly intensified warming region is centered at Japan, and the warming began to enhance since 1940s, which was likely caused by the rapid industrial development in this period.

The 5th IC depicts the cooling phenomenon at the equatorial cold tongue. The time series is quite similar to the global temperature change (Hansen et al., 2010). As suggested by Zhang et al. (2010), this mode is likely driven by global warming.

3.3 *Relationships between the variability of the SCS-SSH and the Pacific oscillations*

In this section, we examine the relationship between the spa-

tio-temporal variability of the SCS-SSH and the Pacific oscillations based on the above analysis. The PC1 (Fig. 3) and PC2 (Fig. 4) are the two time series that characterize the major variability of the SCS-SSH. Therefore, we simply examine their relationship with ENSO, PDO, and the five independent oscillation modes (Fig. 6).

It is straightforward to relate the two PCs of the SCS-SSH with ENSO and PDO indices as they exhibit interannual and near-decadal oscillations respectively. As shown in Fig. 5b, the PC1 and the ENSO index are negatively correlated, especially in the year 1997/1998, when the ENSO index reaches to maximum and the PC1 is at its minimum. The correlation coefficient between them is –0.60, suggesting that the annual cycle of the SCS-SSH is modulated by ENSO, with the amplitude being damped during El Niño period while enhanced during La Niña period. The PC2 is closely related with the PDO index (Fig. 5c) as the former being in good agreement with the latter PDO index, having the correlation coefficient between them as high as 0.87.

The effects of the independent Pacific oscillations (Fig. 6) on the low frequency variability of the SCS-SSH are also examined. Here, the second PC of the CSEOF mode of the SCS-SSH (PC2) is taken as an index that characterize the low frequency variability of the SSH in the SCS; the corresponding spatial pattern is shown in Fig. 4. Each IC is compared with the PC2 and their correlation is calculated (Fig. 7). An interesting result is that the classical ENSO variability mode (1st IC) has little effect on the low frequency variability mode of the SCS-SSH, while the ENSO reddening mode (2nd IC) has a clear effect on that (Fig. 7). This result helps explain why the PDO is more important than ENSO in modulating the low frequency variability of the SCS-SSH, as the ENSO reddening mode (similar to CP ENSO mode) is an important constituent for the PDO.

Based on the above analysis, we can hypothesize that the purely ENSO mode is likely to have an effect on the low frequency variability of the SST in the SCS (SCS-SST) (indicated by the 1st IC spatial mode) other than that of the SCS-SSH, while the ENSO reddening mode can have an effect on the low frequency variability of the SCS-SSH other than that of the SCS-SST.

4 Conclusions and discussion

By applying the CSEOF method, the spatio-temporal variability modes of the SCS-SSH are detected from observed data. The first CSEOF mode represents the annual cycle of the SCS-SSH that is modulated by a low frequency oscillation, which is negatively correlated with the ENSO index. The annual cycle of the SCS-SSH gets reduced during El Niño events, while gets enhanced during La Niña events. The second CSEOF mode represents the low frequency oscillation of the SCS-SSH, which is mostly related to PDO; the spatial response to low frequency modulation is relatively seasonally independent. These results suggest that ENSO and PDO are playing different roles in modulating the spatio-temporal variability of the SSH in the SCS.

The strength of the annual cycle of the SCS-SSH tends to be influenced by the ENSO. To test whether that of the SCS-SST also undergoes a similar variability, we analyzed the HadISST data from 1980 to 2012 in the SCS using the same method. Results are presented in Figs 8 and 9. However, no damped annual cycle can be clearly seen in El Niño periods (Fig. 8); the correlation between PC1 of SCS-SST and ENSO index is –0.25. On the contrary, the SST in the Tropical Pacific (TP-SST) has been reported to display a reduced annual cycle during the El Niño periods (Kim and Chung, 2001). We analyzed the SST in the same domain (20°S–20°N, 124°E–70°W) from 1980 to 2012 using the CSEOF method and reproduced their results, with 70% and 16% of the total variance being explained from the first two modes (the two PCs are shown in Figs 10a and b respectively). It is envi-

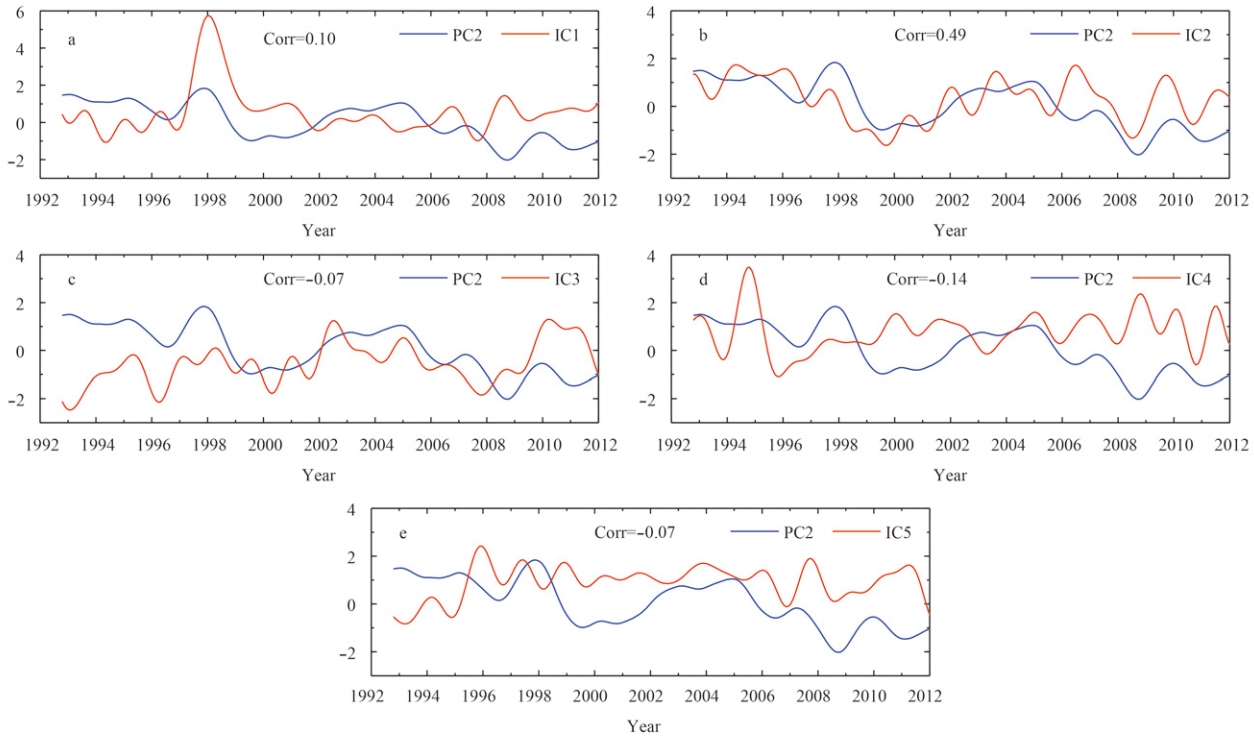

Fig. 7. Comparison of the independent components in the Pacific basin and the low frequency variability mode of the SCS-SSH (as characterized by PC2, see Fig. 4).

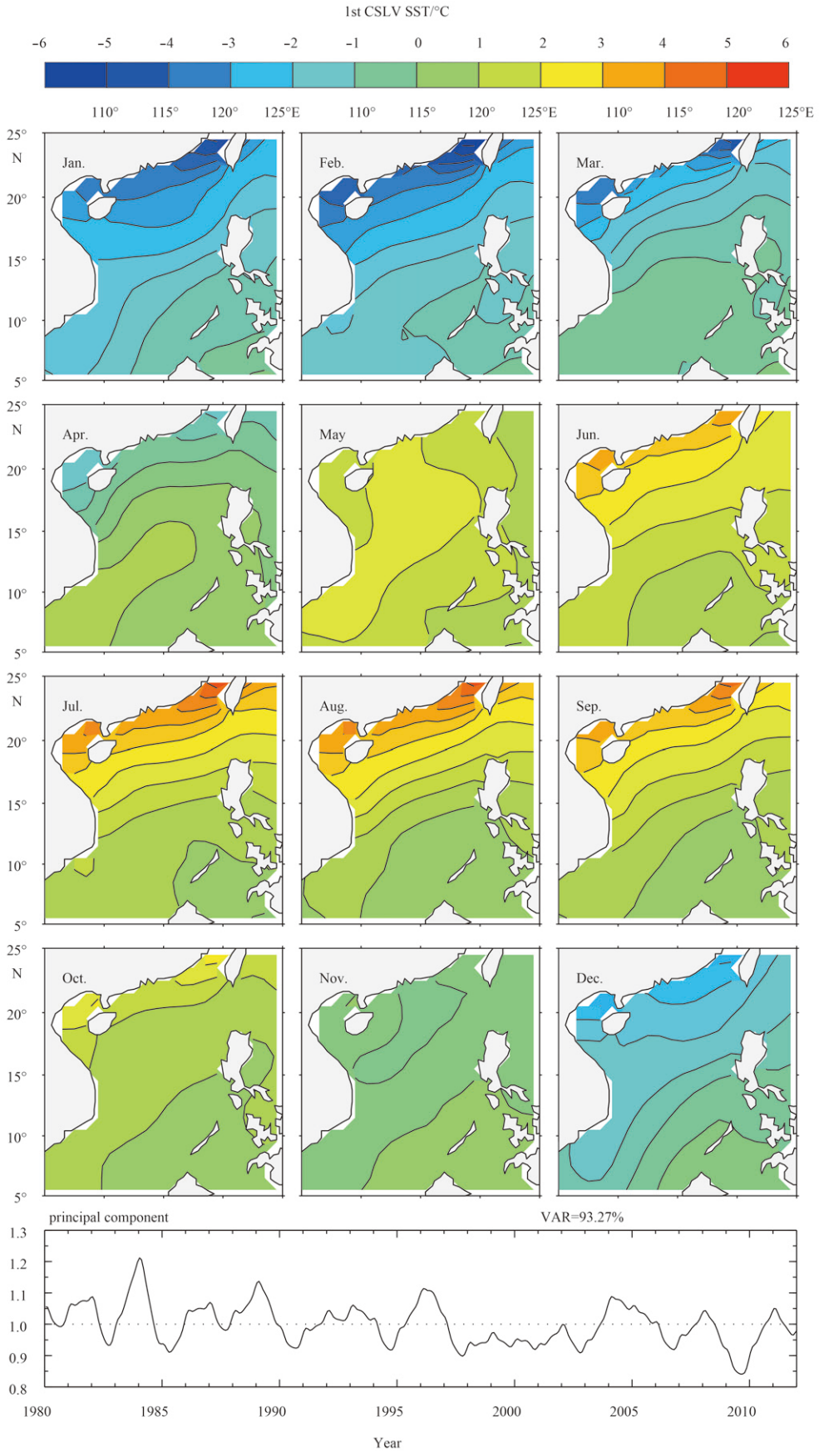

Fig. 8. The first CSEOF mode of SST in the SCS. The 12-month spatial patterns represent a cyclostationary loading vector, while the black line displayed at the bottom panel represents the principal component.

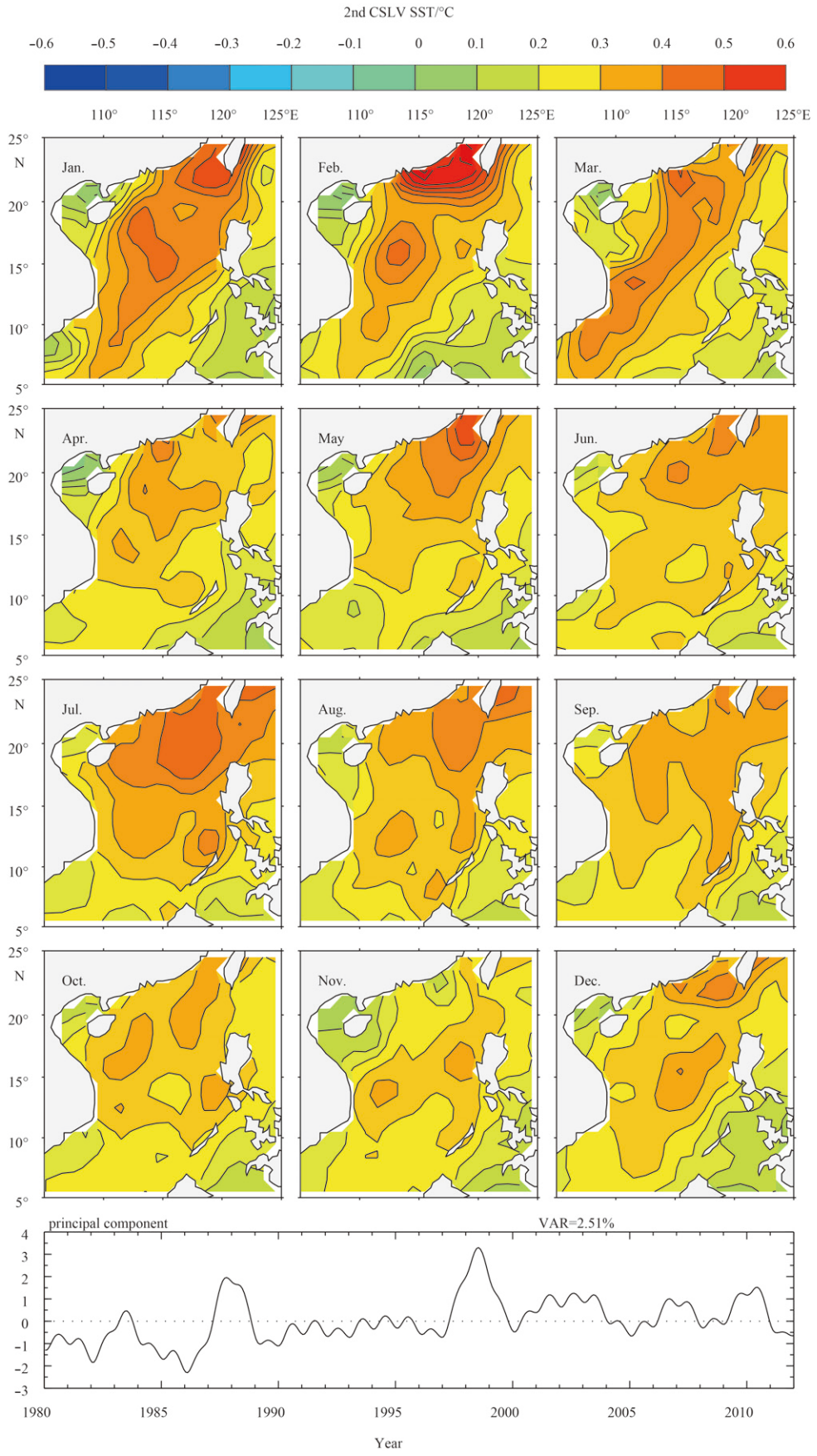

Fig. 9. The second CSEOF mode of SST in the SCS. The 12-month spatial patterns represent a cyclostationary loading vector, while the black line displayed at the bottom panel represents the principal component.

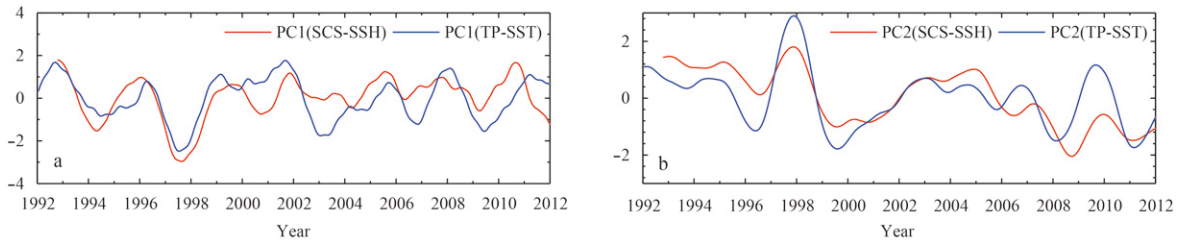

Fig. 10. Comparison of the first (a) and the second (b) PCs of the SCS-SSH and that of the tropical Pacific SST (TP-SST).

sioned that the first two PCs of TP-SST have similar variability pattern with that of the SCS-SSH, suggesting that there are probably some connections between the variability modes of the SCS-SSH and the TP-SST. That means the variability modes of SSH in the SCS is more closely related to the SST variability in the tropical Pacific other than that in the SCS.

On the low frequency variability mode of the SCS-SSH, the PDO tends to play a more important role than ENSO. This result is in agreement with that reported by Wu (2013). To strengthen this conclusion, the SSH footprints of ENSO and PDO are compared with each other. Figures 11a and b show the regression coefficient maps of the SSH against the ENSO and PDO indices. Compared to the ENSO's footprint (Fig. 11a), the PDO's footprint (Fig. 11b) is characterized by an intensification of a low anomaly in the mid-latitudes, and the westward shifts of a high anomaly in the eastern tropics and a low anomaly in the western tropics.

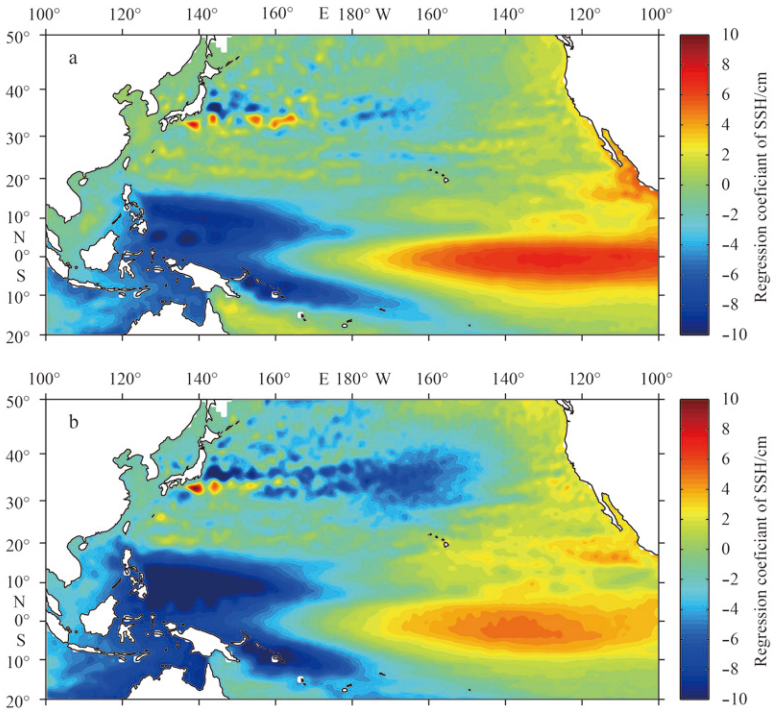

Fig. 11. Maps of regression coefficients of the SSH against ENSO and PDO respectively.

Similar results were also reported by Zhang and Church (2012). It is clear that the PDO's effect can penetrate into the SCS more than that of the ENSO. By comparing the low frequency variability mode of the SCS-SSH with the ICs in the Pacific, it is found that the purely ENSO-like mode (1st IC) has less effect on the low frequency variability of the SCS-SSH, even it is important for that of the SCS-SST. On the contrary, the ENSO-reddening mode (2nd IC) has a clear effect on the low frequency variability of the SCS-SSH, even it is of little importance for that of the SCS-SST. As the ENSO-reddening mode is an important constituent of PDO (e.g., Newman et al., 2003), this explains why the PDO is more important than ENSO in modulating the low frequency variability of the SCS-SSH.

It is likely that the Pacific oscillations are influencing the SCS-SSH and SCS-SST in different ways. The low frequency variability of the SCS-SSH is significant in the southeast of the SCS as revealed from its second CSLV (Fig. 4), while that of the SCS-SST (Fig. 9) is significant in the northern SCS. This difference implies that the SSH and SST in the SCS is likely impacted by different Pacific oscillations, or in different ways. It is identified that the low frequency variability of the SCS-SST is mostly influenced by the purely ENSO mode, while that of the SCS-SSH is mostly influenced by the ENSO-reddening mode (with the effect being probably transferred by planetary waves from the ocean tunnel; see Liu et al., 2011).

Acknowledgements

We would like to thank Chen Dake and Su Jilan for the inspirations and supports to the authors. The constructive comments from two anonymous reviewers are also greatly appreciated. The altimeter products were produced by Ssalto/Duacs and distributed by Aviso, with support from Cnes (http://www.aviso.altimetry.fr/duacs/). The HadISST data are downloaded from the Met Office Hadley Centre (http://www.metoffice.gov.uk/hadobs/). The Fortran 90 subroutine of CSEOF decomposition was created by Dave Stepaniak (who worked for NCAR's Research Data Archive) and downloaded from http://www.cgd.ucar.edu/cas/software/. The FastICA package was downloaded from the Department of Information and Computer Science, School of Science, Aalto University (http://research.ics.aalto.fi/ica/fastica/code/dlcode.shtml).

References

Aires F, Rossow W B, Chédin A. 2002. Rotation of EOFs by the independent component analysis: toward a solution of the mixing problem in the decomposition of geophysical time series. J Atmos Sci, 59: 111–123

Alexander M A, Bladé I, Newman M, et al. 2002. The atmospheric bridge: the Influence of ENSO teleconnections on air-sea interaction over the global oceans. J Climate, 15: 2205–2231

Ashok K, Behera S K, Rao S A, et al. 2007. El Niño Modoki and its possible teleconnection. J Geophys Res, 112: C11007, doi: 10.1029/2006JC003798

Cane M A, Clement A C, Kaplan A, et al. 1997. Twentieth-century sea surface temperature trends. Science, 275: 957–960

Chao S Y, Shaw P T, Wu S Y. 1996. El Niño modulation of the South China Sea circulation. Progress in Oceanography, 38: 51–93

Deser C, Phillips A S, and Alexander M A. 2010. Twentieth century tropical sea surface temperature trends revisited, Geophys Res Lett, 37: L10701, doi: 10.1029/2010GL043321

Fang Guohong, Chen Haiying, Wei Zexun, et al. 2006. Trends and interannual variability of the South China Sea surface winds, surface height, and surface temperature in the recent decade. J Geophys Res, 111: C11S16, doi: 10.1029/2005JC003276

Hannachi A, Unkel S, Trendafilov N T, et al. 2009. Independent component analysis of climate data: a new look at EOF rotation. J Climate, 22: 2797–2812

Hansen J, Ruedy R, Sato M, et al. 2010. Global surface temperature change. Rev Geophys, 48: RG4004, doi: 10.1029/2010RG000345

Ho C R, Zheng Quanan, Soong Y S, et al. 2000. Seasonal variability of sea surface height in the South China Sea observed with TOPEX/Poseidon altimeter data. J Geophys Res, 105(C6): 13981–13990

Hu Jianyu, Kawamura H, Hong Huasheng, et al. 2000. A review on the currents in the South China Sea: Seasonal circulation, South China Sea warm current and Kuroshio intrusion. J Oceanogr, 56: 607–624

Hyvärinen A, Oja E. 2000. Independent component analysis: algorithms and applications. Neural networks, 13(4): 411–430

Kao H Y, Yu Jin-Yi. 2009. Contrasting eastern-Pacific and central-Pacific types of ENSO. J Climate, 22: 615–632

Kim K Y, Chung C. 2001. On the evolution of the annual cycle in the tropical Pacific. Journal of Climate, 14: 991–994

Kim K Y, North G R. 1997. EOFs of harmonizable cyclostationary processes. J Atmos Sci, 54: 2416–2427

Kim K Y, Wu Qigang. 1999. A comparison study of EOF techniques: Analysis of nonstationary data with periodic statistics. J Climate, 12: 185–199

Kug J S, Jin Fei-Fei, An S I. 2009. Two types of El Niño events: cold tongue El Niño and warm pool El Niño. J Climate, 22: 1499–1515

Lau N C, Nath M J. 1996. The role of the "Atmospheric Bridge" in linking tropical Pacific ENSO events to extratropical SST anomalies. J Climate, 9: 2036–2057

Liu Qinyan, Feng Ming, Wang Dongxiao. 2011. ENSO-induced interannual variability in the southeastern South China Sea. J Oceanogr, 67: 127–133

Mantua N J, Hare S R, Zhang Yuan, et al. 1997. A Pacific interdecadal climate oscillation with impacts on salmon production. Bull Am Meteorol Soc, 78(6): 1069–1079

Meyers S D, O'Brien J J, Thelin E. 1999. Reconstruction of monthly SST in the Tropical Pacific Ocean during 1868–1993 using adaptive climate basis functions. Mon Wea Rev, 127: 1599–1612

Newman M, Compo G P, Alexander M A. 2003. ENSO-forced variability of the Pacific decadal oscillation. J Climate, 16(23): 3853–3857

North G R. 1984. Empirical orthogonal functions and normal modes. J Atmos Sci, 41(5): 879–887

Qiu Bo, Lukas R. 1996. Seasonal and interannual variability of the North Equatorial Current, the Mindanao Current and the Kuroshio along the Pacific western boundary. J Geophys Res, 101(C5): 12315–12330

Qiu Fuwen, Fang Wendong, Fang Yue, et al. 2012. Anomalous oceanic characteristics in the South China Sea associated with the large-scale forcing during 2006–2009. Journal of Marine Systems, 100–101: 9–18

Qu Tangdong, Kim Y Y, Yaremchuk M, et al. 2004. Can Luzon Strait transport play a role in conveying the impact of ENSO to the South China Sea?. J Climate, 17: 3644–3657

Rayner N A, Parker D E, Horton E B, et al. 2003. Global analyses of sea surface temperature, sea ice, and night marine air temperature since the late nineteenth century. J Geophys Res, 108(D14), 4407, doi: 10.1029/2002JD002670

Su Jilan. 2004. Overview of the South China Sea circulation and its influence on the coastal physical oceanography outside the Pearl River Estuary. Continental Shelf Research, 24: 1745–1760

Wang Bin, An S I. 2005. A method for detecting season-dependent modes of climate variability: S-EOF analysis. Geophys Res Lett, 32: L15710, doi: 10.1029/2005GL022709

Wang Dongxiao, Liu Qinyan, Huang Rui-Xin, et al. 2006. Interannual variability of the South China Sea throughflow inferred from wind data and an ocean data assimilation product. Geophys Res Lett, 33: L14605, doi: 10.1029/2006GL026316

Wu C R. 2013. Interannual modulation of the Pacific Decadal Oscillation (PDO) on the low-latitude western North Pacific. Progress in Oceanography, 110:49–58

Wu C R, Shaw P T, Chao S Y. 1998. Seasonal and interannual variations in the velocity field of the South China Sea. J Oceanogr, 54: 361–372

Wu Lixin, Cai Wenju, Zhang Liping, et al. 2012. Enhanced warming over the global subtropical western boundary currents. Nature Climate Change, 2: 161–166

Zhang Rong-Hua, Levitus S. 1997. Structure and cycle of decadal variability of upper-ocean temperature in the North Pacific. J Climate, 10: 710–727

Zhang Rong-Hua, Rothstein L M, Busalacchi A J. 1998. Origin of upper-ocean warming and El Niño change on decadal scales in the tropical Pacific Ocean. Nature, 391: 879–883

Zhang Wenjun, Li Jianping, Zhao Xia. 2010. Sea surface temperature cooling mode in the Pacific cold tongue. J Geophys Res, 115: C12042, doi: 10.1029/2010JC006501

Zhang Xuebin, Church J A. 2012. Sea level trends, interannual and decadal variability in the Pacific Ocean. Geophys Res Lett, 39: L21701, doi: 10.1029/2012GL053240

Zhang Yuan, Wallace J M, Battisti D S. 1997. ENSO-like interdecadal variability: 1900–93. J Climate, 10: 1004–1020

Zheng Zhe-Wen, Ho C R, Kuo N J. 2007. Mechanism of weakening of west Luzon eddy during La Niña years. Geophys Res Lett, 34: L11604, doi: 10.1029/2007GL030058

Zhou Jian, Li Peiliang, Yu Haili. 2012. Characteristics and mechanisms of sea surface height in the South China Sea. Global and Planetary Change, 88–89: 20–31

Zhu Jieshun, Huang Bohua, Wu Zhaohua. 2012. The role of ocean dynamics in the interaction between the Atlantic meridional and equatorial modes. J Climate, 25: 3583–3598